One-electron self-energies and spectral functions for the *t-J* model in the large-*N* limit

M. Bejas, A. Greco, and A. Foussats
Facultad de Ciencias Exactas, Ingeniería y Agrimensura and Instituto de Física Rosario (UNR-CONICET), Avenida Pellegrini 250-2000 Rosario, Argentina
(Received 14 February 2006; published 8 June 2006)

Using a recently developed perturbative approach, which considers Hubbard operators as fundamental excitations, we have performed electronic self-energy and spectral function calculations for the *t-J* model on the square lattice. We have found that the spectral functions along the Fermi surface are isotropic, even close to the critical doping where the *d* density wave phase occurs. Fermi liquid behavior with scattering rate $\sim\omega^2$ and a finite quasiparticle weight Z was obtained. Z decreases with decreasing doping taking low values for low doping. Results are compared with others obtained by analytical and numerical methods like the slave-boson and Lanczos diagonalization approaches, finding agreement. We discuss our results in the light of recent angle-resolved photoemission spectroscopy experiments in cuprates.

DOI: 10.1103/PhysRevB.73.245104 PACS number(s): 71.10.Fd, 71.27.+a

I. INTRODUCTION

Since the discovery of high-T_c superconductivity[1] a large part of the solid state community has accepted that the *t-J* model is fundamental for understanding the physics of cuprates.[2] However, in spite of the great deal of work done, important questions about this model are still open; the one-electron spectral function being one of the most relevant. The recent improvement of angle-resolved photoemission spectroscopy (ARPES) experiments has allowed access to more refined information about one-electron spectral functions and self-energy effects,[3] both considered relevant for understanding the physics of cuprates.

The main problem in calculating spectral properties in the framework of the *t-J* model is the treatment, in a controllable way, of the non-double-occupancy constraint. There are several analytical and numerical approaches used to treat the constrained algebra of the *t-J* model. We will mention some of them. On the analytical side the following methods are in use. (a) The self-consistent Born approximation[4] is appropriate for the one-hole problem. (b) The slave-fermion (SF) method;[5] it is accepted that the method is reasonable for low doping, but there are not many calculations of spectral functions which require the evaluation of fluctuations above the mean-field level. (c) The slave-boson (SB) method,[5] unlike the SF, seems to be appropriate for describing the metallic regime. However, like the SF method, the treatment of fluctuations above the mean field is not trivial (we further discuss this point below). From the numerical side can be mentioned (a) the quantum Monte Carlo (QMC) method, which is suitable for calculating spectral functions for the one-hole case[6] while for finite doping the sign problem makes the calculation uncontrolled; and (b) Lanczos diagonalization[7] and its finite-temperature version,[8] which are limited to finite clusters. Thus, there is no single method covering all situations; therefore it is important to complement analytical with numerical methods and vice versa.

In Ref. 9 we developed, for $J=0$, a perturbative large-N approach for the *t-J* model based on the path integral representation for Hubbard operators (or X operators) which, in what follows, will be called the PIH method. This method deals with X operators as fundamental objects and is not based on any decoupling scheme; thus, there are no complications of gauge fixing and Bose condensation as in the SB approach.[10] Recently,[11] the PIH approach was extended to the case of finite J. The obtained phase diagram and charge correlations were compared with other calculations based on the SB (Ref. 12) and Bayn-Kadanoff functional theory,[13] finding good agreement.

The aim of the present paper is to present the one-particle spectral function and self-energy calculations using the PIH approach. We show that the method is useful for explicit calculation of spectral properties, enabling us to sum up, systematically, fluctuations above the mean-field solution, giving reliable results.

The paper is organized as follows. In Sec. II, after a brief summary of the PIH method, we show the analytical expressions for the self-energy and the spectral function. In Sec. III, the results are compared with available SB ones. In Sec. IV, the results are compared with Lanczos diagonalization ones for different $\mathbf{k}$'s on the Brillouin zone (BZ) and different doping levels. In Sec. V we present a detailed analysis for self-energies and spectral functions for several doping levels and J. Conclusions and discussions are given in Sec. VI.

II. BRIEF SUMMARY OF THE FORMALISM: SELF-ENERGY AND SPECTRAL FUNCTION CALCULATION

The PIH approach was developed extensively in previous papers[9,11,14,15] and in this section we list the main useful steps for explicit calculations of the self-energy and spectral functions.

We associate with the N-component fermion field f_p the propagator, connecting two generic components p and p',

$$G^{(0)}_{pp'}(\mathbf{k},\omega_n) = -\frac{\delta_{pp'}}{i\omega_n - E_k} \tag{1}$$

which is $O(1)$. The original spin index $\sigma=\pm$ was extended to the index p running from 1 to N.

The fermion variable f_{ip} is proportional to the fermionic X operator X_i^{0p}, $f_{ip}=(1/\sqrt{N}r_0)X_i^{0p}$, and cannot be associated with the spinons as in the SB approach. In Eq. (1), E_k $[E_k=-2(tr_0+\Delta)(\cos k_x+\cos k_y)-\mu]$ is the electronic dispersion in leading order, where t is the hopping between nearest-neighbor sites on the square lattice and μ the chemical potential. The mean-field values r_0 and Δ must be determined by minimizing the leading-order theory. From the completeness condition $(\Sigma_p X_i^{pp}+X_i^{00}=N/2)$, r_0 is equal to $\delta/2$ where δ is the hole doping away from half filling. The expression for Δ is

$$\Delta=\frac{J}{2N_s}\sum_k \cos(k_x)n_F(E_k) \tag{2}$$

where n_F is the Fermi function, J is the exchange interaction between nearest-neighbors, and N_s is the number of sites in the BZ. For a given doping δ, μ and Δ must be determined self-consistently from $(1-\delta)=\frac{2}{N_s}\Sigma_k n_F(E_k)$ and Eq. (2).

We associate with the six-component boson field $\delta X^a=(\delta R,\delta\lambda,r^x,r^y,A^x,A^y)$ the inverse of the propagator connecting two generic components a and b,

$$D^{-1}_{(0)ab}(\mathbf{q},\nu_n)=N\begin{pmatrix} -2Jr_0^2[\cos(q_x)+\cos(q_y)] & r_0 & 0 & 0 & 0 & 0\\ r_0 & 0 & 0 & 0 & 0 & 0\\ 0 & 0 & \frac{4}{J}\Delta^2 & 0 & 0 & 0\\ 0 & 0 & 0 & \frac{4}{J}\Delta^2 & 0 & 0\\ 0 & 0 & 0 & 0 & \frac{4}{J}\Delta^2 & 0\\ 0 & 0 & 0 & 0 & 0 & \frac{4}{J}\Delta^2 \end{pmatrix}. \tag{3}$$

The bare boson propagator $D^{(0)}_{ab}$ is $O(1/N)$. The first component δR of the δX^a field is related to the charge fluctuations by $X_i^{00}=Nr_0(1+\delta R_i)$, where X^{00} is the Hubbard operator associated with the number of holes. $\delta\lambda$ is the fluctuation of the Lagrangian multiplier λ_i associated with the completeness condition. r_i^η and A_i^η correspond, respectively, to the amplitude and the phase fluctuations of the bond variable $\Delta_i^\eta=\Delta(1+r_i^\eta+iA_i^\eta)$ where $\eta=x,y$.

The three-leg vertex

$$\begin{aligned}\Lambda_a^{pp'}=(-1)\Bigg[&\frac{i}{2}(\omega_n+\omega'_n)+\mu+2\Delta\\ &\times\sum_\eta \cos\left(k_\eta-\frac{q_\eta}{2}\right)\cos\frac{q_\eta}{2};1;\\ &-2\Delta\cos\left(k_x-\frac{q_x}{2}\right);-2\Delta\cos\left(k_y-\frac{q_y}{2}\right);2\Delta\\ &\times\sin\left(k_x-\frac{q_x}{2}\right);2\Delta\sin\left(k_y-\frac{q_y}{2}\right)\Bigg]\delta^{pp'}\end{aligned} \tag{4}$$

represents the interaction between two fermions and one boson.

The four-leg vertex $\Lambda_{ab}^{pp'}$ represents the interaction between two fermions and two bosons. The only elements different from zero are

$$\begin{aligned}\Lambda_{\delta R\delta R}^{pp'}=\Bigg[&\frac{i}{2}(\omega_n+\omega'_n)+\mu+\Delta\sum_\eta \cos\left(k_\eta-\frac{q_\eta+q'_\eta}{2}\right)\\ &\times\left(\cos\frac{q_\eta}{2}\cos\frac{q'_\eta}{2}+\cos\frac{q_\eta+q'_\eta}{2}\right)\Bigg]\delta^{pp'},\end{aligned} \tag{5}$$

$$\Lambda_{\delta R\delta\lambda}^{pp'}=\frac{1}{2}\delta^{pp'}, \tag{6}$$

$$\Lambda_{\delta Rr\eta}^{pp'}=-\Delta\cos\left(k_\eta-\frac{q_\eta+q'_\eta}{2}\right)\cos\frac{q'_\eta}{2}\delta^{pp'}, \tag{7}$$

and

$$\Lambda_{\delta RA\eta}^{pp'}=\Delta\sin\left(k_\eta-\frac{q_\eta+q'_\eta}{2}\right)\cos\frac{q'_\eta}{2}\delta^{pp'}. \tag{8}$$

Each vertex conserves the momentum and energy and they are $O(1)$. In each diagram there is a minus sign for each fermion loop and a topological factor. A brief summary of the Feynman rules is given in Fig. 1(a). As usual in a large-N approach, any physical quantity can be calculated at a given order just by counting the powers in $1/N$ of vertices and propagators involved in the corresponding diagrams.

The bare boson propagator $D^{(0)}_{ab}$ is renormalized in $O(1/N)$. From the Dyson equation, $(D_{ab})^{-1}=(D^{(0)}_{ab})^{-1}-\Pi_{ab}$, the dressed components D_{ab} [double-dashed line in Fig. 1(b)]

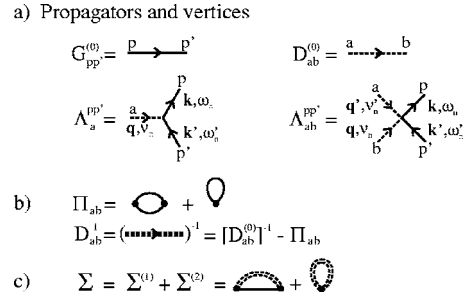

FIG. 1. (a) Summary of the Feynman rules. Solid line represents the propagator $G^{(0)}$ [Eq. (1)] for the correlated fermion f_p. Dashed line represents the 6×6 boson propagator $D^{(0)}$ [Eq. (3)] for the six-component field δX^a. Note that the component (1,1) of this propagator is directly associated with the X^{00} charge operator. $\Lambda_a^{pp'}$ [Eq. (4)] and $\Lambda_{ab}^{pp'}$ represent the interaction between two fermions f_p and one and two bosons δX^a, respectively. (b) Π_{ab} contributions to the irreducible boson self-energy. (c) Contributions to the electron self-energy $\Sigma(\mathbf{k},\omega)$ through $O(1/N)$.

of the boson propagator can be found after evaluating the 6×6 boson self-energy matrix Π_{ab}. Π_{ab} may be evaluated by Feynman rules through the diagrams in Fig. 1(b).

In the present summary there is no mention of the ghost fields. They were already treated in previous papers and the only role they play is to cancel the infinities given by the two diagrams shown in Fig. 1(b).

From the N-extended completeness condition it may be seen that the charge operator X^{00} is $O(N)$, while the operators X^{pp} are $O(1)$. This fact will have the physical consequence that the PIH approach weakens the effective spin interaction compared to the one related to the charge degree of freedom.

The component D_{RR} [component (1,1)] of the 6×6 boson propagator is related to the charge-charge correlation function χ^c by

$$\chi^c(q,\nu_n)=N\left(\frac{\delta}{2}\right)^2 D_{RR}(q,\nu_n). \tag{9}$$

In Refs. 9 and 11 we have pointed out that, in $O(1)$, the charge-charge correlation function shows the presence of collective peaks above the particle-hole continuum.

In what follows self-energies and one-particle spectral functions are calculated by means of the Feynman rules. The Green's function (1) corresponds to the N-infinite propagator which includes no dynamical corrections; these appear at higher order in the $1/N$ expansion. For obtaining spectral densities, the self-energy Σ is calculated. Using the Feynman rules, the total self-energy in $O(1/N)$ is obtained by adding the contribution of the two diagrams shown in Fig. 1(c). The analytical expression for Σ, for a given channel p, is

$$\Sigma(\mathbf{k},i\omega_n)=\Sigma^{(1)}(\mathbf{k},i\omega_n)+\Sigma^{(2)}(\mathbf{k},i\omega_n), \tag{10}$$

where

$$\Sigma^{(1)}(\mathbf{k},i\omega_n)=\frac{1}{N_s}\sum_{\mathbf{q},\nu_n}\Lambda_a^{pp}D_{ab}(\mathbf{q},i\nu_n)\times G_{pp}^{(0)}(\mathbf{k}-\mathbf{q},i(\omega_n-\nu_n))\Lambda_b^{pp}, \tag{11}$$

and

$$\Sigma^{(2)}(\mathbf{k},i\omega_n)=\frac{1}{N_s}\sum_{\mathbf{q},\nu_n}\Lambda_{ab}^{pp}D_{ab}(\mathbf{q},i\nu_n). \tag{12}$$

The sum over repeated indices a and b is assumed. The renormalized boson propagator D_{ab} plays a similar role to the phonon propagator when dealing with the electron-phonon interaction in simple metals. Therefore, in the calculation of $\Sigma(\mathbf{k},\omega)$ through $O(1/N)$, band structure effects and collective effects associated with the charge degrees of freedom are involved [see Eq. (9)]. Using the spectral representation for the boson field D_{ab}, we obtain

$$\Sigma^{(1)}(\mathbf{k},i\omega_n)=\frac{1}{2\pi N_s}\int d\nu\sum_{\mathbf{q},\nu_n}\Lambda_a^{pp}\frac{B^{ab}(\mathbf{q},\nu)}{i\nu_n-\nu}\Lambda_b^{pp}\times G_{pp}^{(0)}(\mathbf{k}-\mathbf{q},i(\omega_n-\nu_n)), \tag{13}$$

$$\Sigma^{(2)}(\mathbf{k},i\omega_n)=\frac{1}{2\pi N_s}\int d\nu\sum_{\mathbf{q},\nu_n}\Lambda_{ab}^{pp}\frac{B^{ab}(\mathbf{q},\nu)}{i\nu_n-\nu}, \tag{14}$$

where

$$B^{ab}(\mathbf{q},\nu)=-2\lim_{\eta\to0}\mathrm{Im}[D_{ab}(\mathbf{q},i\nu_n\to\nu+i\eta)]. \tag{15}$$

After performing the Matsubara sum and the analytical continuation $i\omega_n=\omega+i\eta$, the imaginary part of Σ is

$$\mathrm{Im}\,\Sigma(\mathbf{k},\omega)=\frac{1}{2N_s}\sum_{\mathbf{q}}h_a(k,q,\omega-E_{k-q})\,B^{ab}(\mathbf{q},\omega-E_{k-q})h_b(k,q,\omega-E_{k-q})\times[n_F(-E_{k-q})+n_B(\omega-E_{k-q})] \tag{16}$$

where n_B is the Bose factor, and the six-component vector $h_a(k,q,\nu)$ is

$$h_a(k,q,\nu)=\left[\frac{2E_{k-q}+\nu+2\mu}{2}+2\Delta\sum_{\eta}\cos\left(k_\eta-\frac{q_\eta}{2}\right);1;-2\Delta\cos\left(k_x-\frac{q_x}{2}\right);-2\Delta\cos\left(k_y-\frac{q_y}{2}\right);2\Delta\sin\left(k_x-\frac{q_x}{2}\right);2\Delta\sin\left(k_y-\frac{q_y}{2}\right)\right].$$

It is interesting to show the more compact result for the case $J=0$:

$$\mathrm{Im}\,\Sigma(\mathbf{k},\omega)=\frac{1}{2N_s}\sum_{\mathbf{q}}[\Omega^2B^{RR}(\mathbf{q},\omega-E_{k-q})+2\Omega B^{\lambda R}(\mathbf{q},\omega-E_{k-q})+B^{\lambda\lambda}(\mathbf{q},\omega-E_{k-q})]\times[n_F(-E_{k-q})+n_B(\omega-E_{k-q})], \tag{17}$$

where $\Omega=(E_{k-q}+2\mu+\omega)/2$. Using the Kramers-Kronig relations $\mathrm{Re}\,\Sigma(\mathbf{k},\omega)$ can be determined from $\mathrm{Im}\,\Sigma(\mathbf{k},\omega)$ and the

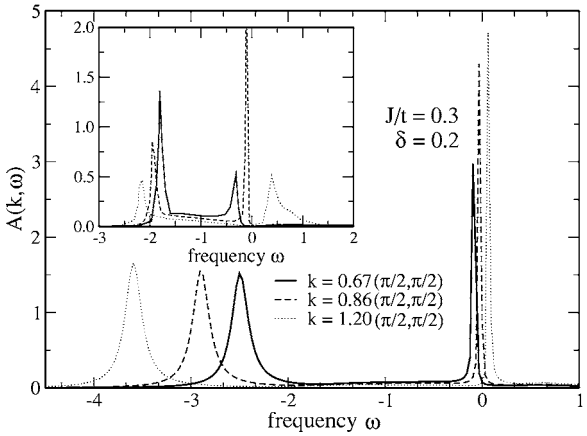

FIG. 2. Solid, dashed, and dotted lines are the spectral functions for $\mathbf{k}=0.67(\pi/2,\pi/2)$, $0.86(\pi/2,\pi/2)$, and $1.2(\pi/2,\pi/2)$, respectively. The frequency ω is in units of t which is considered to be 1. For comparison with the SB approach, in the inset we have included the results from Ref. 16.

spectral function $A(\mathbf{k},\omega)=-\frac{1}{\pi}\,\mathrm{Im}\,G(\mathbf{k},\omega)$ is computed as

$$A(\mathbf{k},\omega)=-\frac{1}{\pi}\frac{\mathrm{Im}\,\Sigma(\mathbf{k},\omega)}{[\omega-E_{\mathbf{k}}-\mathrm{Re}\,\Sigma(\mathbf{k},\omega)]^2+[\mathrm{Im}\,\Sigma(\mathbf{k},\omega)]^2}. \tag{18}$$

The self-energy is calculated using the propagator $G(\mathbf{k},\omega)$ for the f operators, which are proportional to the fermionic Hubbard operators and thus cannot be related to the usual fermions.

III. COMPARISON WITH SLAVE-BOSON METHOD

While many papers on the SB method have been published on the mean-field level there are few calculations including fluctuations above the mean field, which are necessary for the estimation of spectral functions. This shows that, in spite of the popularity of the SB method, it is not trivial to implement this kind of calculations. Even if PIH results have, at the mean-field level, a close connection with the SB results (see Refs. 9 and 11) it is relevant to compare both approaches beyond the mean-field level. To our knowledge, there is only one paper where spectral functions have been calculated in the framework of SB theory.[16] In that paper, the authors present results for $J=0.3$ and doping $\delta=0.20$ for three different $\mathbf{k}$ points on the BZ.

In Fig. 2 we present PIH spectral functions $A(\mathbf{k},\omega)$. The calculation was done for $J=0.3$, $\delta=0.20$, and $\mathbf{k}=0.67(\pi/2,\pi/2)$, $0.86(\pi/2,\pi/2)$, and $1.2(\pi/2,\pi/2)$, which are exactly the same conditions of Fig. 3 in Ref. 16. In the inset of Fig. 2 we have included SB results for comparison. As can be seen, the spectral functions have some similarities with the SB results. We have obtained a low-energy peak and a pronounced structure at large binding energy. The low-energy peak is the quasiparticle (QP). The other features, at large binding energy, are incoherent spectra (IS). For $\mathbf{k}\sim 0.86(\pi/2,\pi/2)$ the QP peak crosses $\omega=0$, where the chemical potential is located. In spite of similarities between the present results and those of Ref. 16 there are some differences. (a) Our IS is located at binding energy larger than that in the SB approach. For instance, for $\mathbf{k}=0.86(\pi/2,\pi/2)$, the IS is at $\omega\sim -3t$ while the corresponding one in the SB method is at $\omega\sim -2t$. (b) Our QP peak is less dispersed than that in the SB approach. As it is well known, self-energy effects depress Fermi velocities (v_F^*) with respect to the bare one (v_F^{bare}), $v_F^*=Zv_F^{bare}$, where $Z=\left(1-\frac{\partial\Sigma}{\partial\omega}\right)$ is the QP weight; therefore, it is concluded that our self-energy effects are larger than those in the SB approach.

In the SB method there are three different Σ's:[16] Σ_n, Σ_a, and Σ_{inc}. In Σ_n, bosons are condensed, in Σ_a one boson is condensed and the other fluctuates, and in Σ_{inc} both bosons fluctuate. These complications are due to the decoupling scheme used in the SB approach, so beyond the mean-field level it is necessary to convolve spinons and bosons to reconstruct the original X operators. As in the PIH approach there is no *a priori* decoupling and we work directly with the Hubbard operators, we have only one self-energy Σ given by Eq. (11). A detailed description of the present self-energies for different δ and J is given in Sec. V.

After comparing spectral functions with some available SB results, in spite of some similarities, we found important differences in the self-energy effects between the two methods. The existence of only a few SB results beyond mean-field level may be closely related to the decoupling scheme which leads to a gauge field theory, making hard the implementation of the approach. We hope that the PIH method will be useful and a complement to the SB calculations.

IV. COMPARISON WITH EXACT DIAGONALIZATION

As pointed out in Sec. II, the PIH approach weakens spin fluctuations compared to charge fluctuations. For instance, at leading order, while there are collective effects in the charge channel, the spin channel exhibits the characteristic form of a Pauli paramagnet where the electronic band is renormalized by correlations.[11,17] Thus, at $O(1/N)$, the self-energy does not contain collective effects, like magnons in the spin channel. Intuitively one may think that the method will be better for large doping than for low doping. However, the exact role played by charge and magnetic excitations as a function of doping, in the t-J model, is one of the key points for understanding the physics of cuprates. Many mechanisms have been proposed. Some of them privilege charge while others privilege magnetism.

In order to test the reliability of our results as a function of doping, in this section, we compare *qualitatively* the present spectral functions with calculations made using Lanczos diagonalization. For this purpose we have performed Lanczos diagonalization[18] on the 4×4 lattice for $\delta=0.75$, 0.5 and 0.3125, with $J=0.3$.

As an example, we will explicitly compare some $\mathbf{k}$ points for several dopings leaving to the reader the analysis of the other $\mathbf{k}$'s.

A. Results for doping $\delta=0.75$

This doping corresponds to 12 holes in the 4×4 lattice. There is good agreement between Lanczos and PIH (Fig. 3)

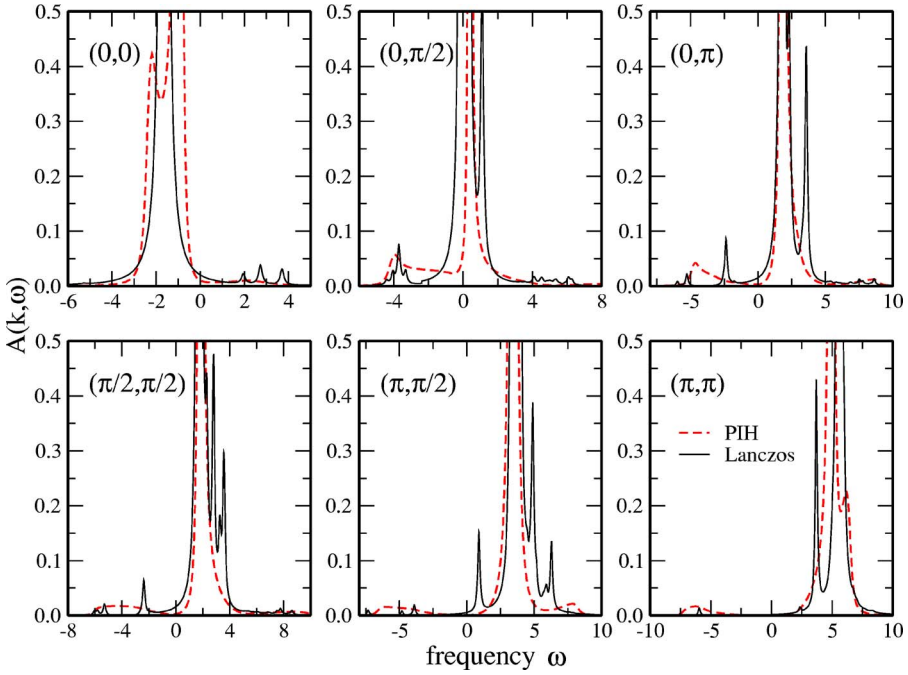

FIG. 3. (Color online) Comparison between spectral function calculations obtained by Lanczos diagonalization for all the allowed **k** points of the 4×4 lattice and results obtained with the PIH method. The parameters are $J=0.3$ and $\delta=0.75$. The **k** points are presented between parentheses in each frame. The frequency ω is in units of t. In order to plot PIH and Lanczos results on the same figure we have used an arbitrary scale for the y axis.

for the six **k** points allowed in the 4×4 lattice. For instance, for $\mathbf{k}=(0,\pi)$ both calculations show a QP peak at around $\omega\sim2t$ and IS at around $\omega\sim-4t$. Lanczos diagonalization shows a small peak at $\omega\sim3t$ which is not seen in the PIH result. However, the PIH result shows an asymmetric shape of the QP peak which can be interpreted as an indication of the additional structure observed in Lanczos diagonalization. For $\mathbf{k}=(0,\pi/2)$ both Lanczos and PIH results show a QP peak near the Fermi level, and IS at $\omega\sim-4t$. The additional peak that appears in the Lanczos result at $\omega\sim1.5t$ can be associated with the nonsymmetrical shape of the QP peak seen in the PIH result.

B. Results for doping $\delta=0.50$

This doping corresponds to eight holes in the 4×4 lattice. Results are presented in Fig. 4 for Lanczos and PIH methods. With decreasing doping from 0.75 to 0.50, both methods show more IS. For instance, for $\mathbf{k}=(0,0)$ both calculations show two well-defined peaks below the Fermi level. The peak closer to the chemical potential is the QP, and the peak near $\omega\sim-3t$ is of incoherent character. Both methods also present small IS for $\omega>0$.

For $\delta=0.5$, results for $J=0$ were presented in Ref. 14 in the context of organic materials where PIH spectral functions were also compared with those obtained using Lanczos di-

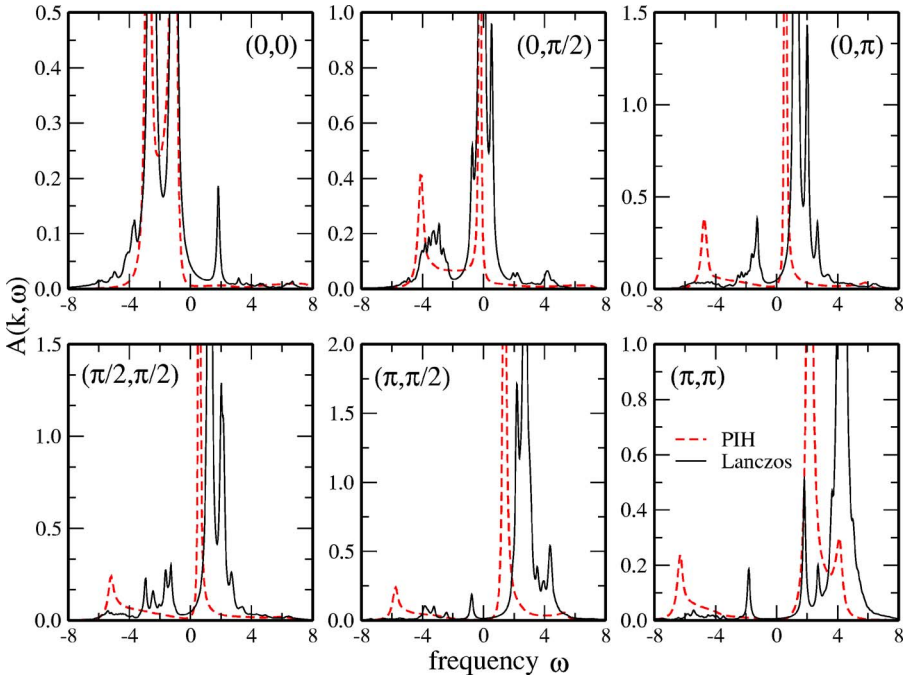

FIG. 4. (Color online) Comparison between spectral function calculations obtained by Lanczos diagonalization for all the allowed **k** points of the 4×4 lattice and results obtained with the PIH method. The parameters are $J=0.3$ and $\delta=0.5$. The **k** points are presented between parentheses in each frame. The frequency ω is in units of t.

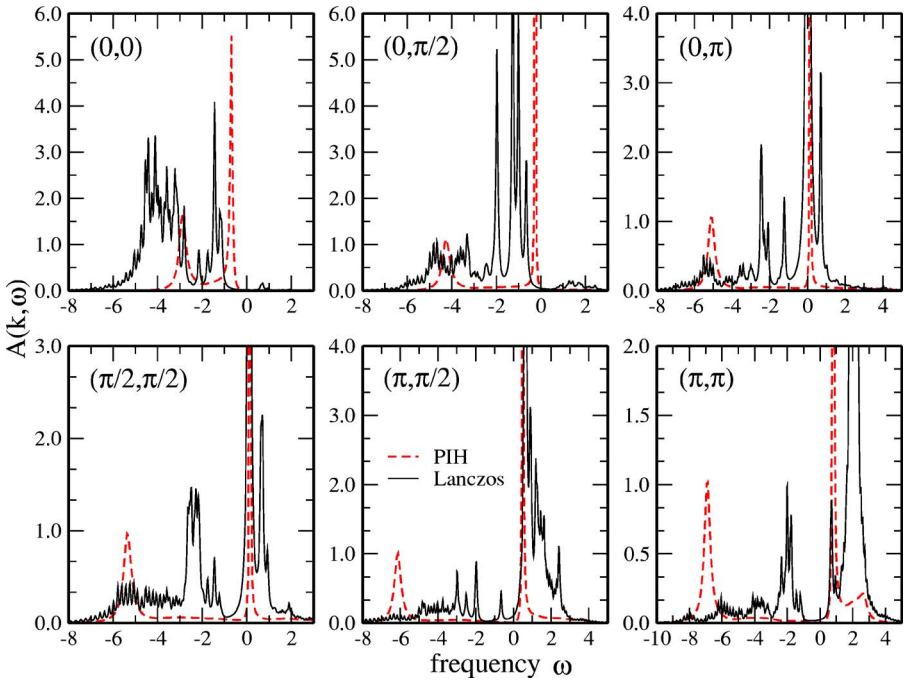

FIG. 5. (Color online) Comparison between spectral function calculations obtained by Lanczos diagonalization for all the allowed **k** points of the 4×4 lattice and results obtained with the PIH method. The parameters are $J=0.3$ and $\delta=0.3125$. The **k** points are presented between parentheses in each frame. The frequency ω is in units of t.

agonalization as a function of the nearest-neighbor Coulomb interaction V.

C. Results for doping $\delta=0.3125$

This doping corresponds to five holes in the 4×4 lattice. The results are presented in Fig. 5 for Lanczos and PIH methods. Both present a QP peak near the Fermi level and stronger IS than for $\delta=0.75$ and 0.5. The increasing of the IS is consistent with the fact that the QP weight is $Z\sim0.5$, lower than for the previous dopings where for $\delta=0.75$ and 0.5 is $Z\sim0.9$ and 0.7, respectively. The QP weight will be discussed in more detail in the next section.

For $\mathbf{k}=(0,0)$ both calculations show a QP peak below the Fermi energy. The peak that appears in the PIH results at $\omega\sim-3t$ is broader in Lanczos diagonalization and centered at $\omega\sim-4t$. For $\mathbf{k}=(\pi,\pi/2)$ both calculations show a QP peak above the Fermi level and the IS on top of this peak. The well-pronounced structure obtained in the PIH method at $\omega\sim-6t$ seems to be missing in the Lanczos result. Instead, it shows a homogeneously distributed IS below the Fermi level up to large binding energies of the order of $-7t$. In the frequency range $-5t<\omega<-1t$ both methods show IS. For $\mathbf{k}=(0,\pi)$ both methods present a QP near the Fermi level and IS at $\omega\sim-5t$. Between those two features it is possible to see IS (in the form of several peaks in Lanczos diagonalization) in both calculations.

For the three studied dopings both methods show that while the QP peak disperses through the Fermi surface (FS), the edge of the IS moves in the opposite direction. This result was obtained previously by Stephan and Horsch.[19] In Ref. 19 the authors also studied spectral functions for the t-J model at moderate doping $\delta\sim0.1$ by means of exact diagonalization. That paper presents strong evidence for a large FS for moderated doping levels. This result gives additional support for our bare band $E_k=-2(t\delta/2+\Delta)(\cos k_x+\cos k_y)-\mu$.

We conclude that the PIH and Lanczos results, for the three studied δ values (which cover a broad range of doping), agree quite well considering the different nature of the two methods. The above comparison gives some confidence in our self-energies. The self-energy has additional information such as relaxation time $1/\tau$, quasiparticle weight Z (effective mass increasing), which cannot be directly obtained from Lanczos diagonalization.

On decreasing doping, Lanczos and PIH methods both show band narrowing. The narrowing is stronger in the PIH than in the Lanczos method. For instance, for $\mathbf{k}=(\pi,\pi)$ (Fig. 4), while the Lanczos QP peak is at $\omega\sim4t$, the PIH QP peak is at $\omega\sim2t$. For $\mathbf{k}=(\pi,\pi)$ (Fig. 5), while the Lanczos QP peak is at $\omega\sim2t$ it is at $\omega\sim1t$ in the PIH method. For $\delta=0.75$ (Fig. 3) there is good agreement in the QP and IS energy positions for each **k**. This discussion is important in the light of ARPES experiments in cuprates[20,21] which show Fermi velocities rather independent of doping (see also Ref. 22 for discussion). In the PIH method the strong narrowing is mainly due to the factor $\delta/2$ in the electronic dispersion which strongly weakens the t term.

V. SELF-ENERGY RENORMALIZATION

In this section, we present a detailed self-energy and spectral function calculations in the PIH method.

Figure 6 shows the QP weight Z as a function of doping for $J=0$. As was shown in Ref. 11, for $J=0$ the homogeneous Fermi liquid (HFL) remains stable for all δ. For each doping, we have found that the self-energy is very isotropic on the FS (see below), making the QP weight rather constant. In Fig. 6 $Z\to0$ when $\delta\to0$. For small δ, $Z\sim1.4\delta$, which is very close to the observed ARPES behavior in LSCO.[23] As Z remains finite for $\delta>0$, present calculation predicts a Fermi liquid (FL) behavior. Figure 6 also shows that $Z\to1$ when

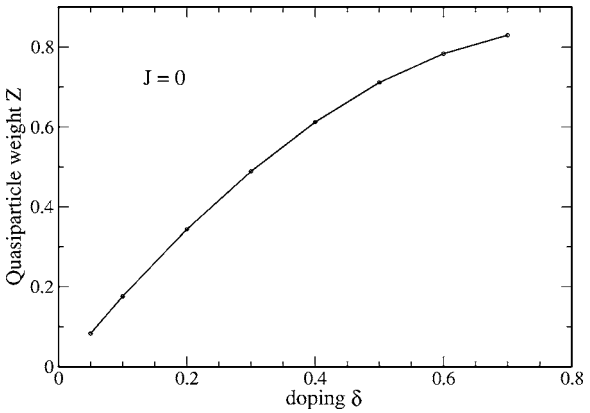

FIG. 6. Quasiparticle weight Z as a function of doping for $J=0$.

$\delta \to 1$ as expected for an uncorrelated system.

Let us discuss the case $J=0.3$. Figure 7 shows Σ, for $\delta=0.3$, for three well-separated $\mathbf{k}$ vectors on the FS. One of the $\mathbf{k}$ is chosen in the (11) direction of the BZ, another in the (10) direction, and the third in between. The top and the middle panels of Fig. 7 show $\mathrm{Im}\,\Sigma$ and $\mathrm{Re}\,\Sigma$, respectively.

As shown in Fig. 7, the PIH method predicts a rather isotropic self-energy on the FS. On the other hand, for each $\mathbf{k}$, $\Sigma(\mathbf{k},\omega)$ is very asymmetric with respect to $\omega=0$ which can be interpreted as a consequence of the difference between addition and removal of a single electron in a correlated system. Near $\omega=0$, $\mathrm{Im}\,\Sigma(\mathbf{k}_F,\omega)\sim\omega^2$, showing FL behavior. On the other hand, $\mathrm{Re}\,\Sigma(\mathbf{k}_F,\omega)$ shows, at $\omega=0$, a negative slope that is also a characteristic of a Fermi liquid.

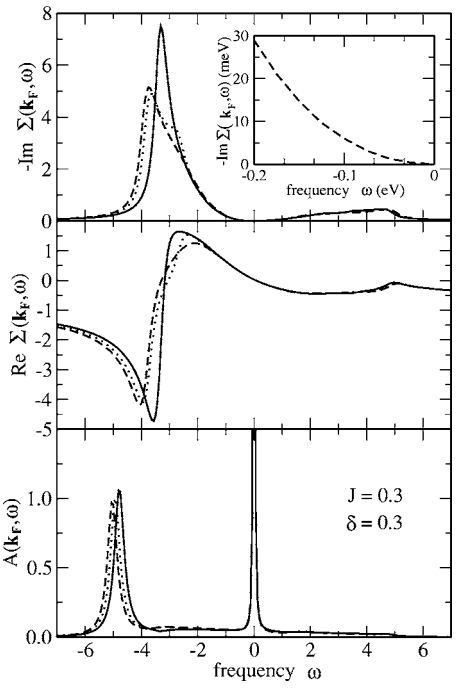

FIG. 7. $-\mathrm{Im}\,\Sigma(\mathbf{k}_F,\omega)$ (top, panel), $\mathrm{Re}\,\Sigma(\mathbf{k}_F,\omega)$ (middle panel), and spectral functions (bottom panel) for $J=0.3$, $\delta=0.30$, and three different points on the FS. Solid, dashed, and dotted lines are results for the Fermi point in the (1,1) and (1,0) directions and between these two, respectively. The frequency ω, $\mathrm{Re}\,\Sigma$, and $\mathrm{Im}\,\Sigma$ are in units of t. Inset: $-\mathrm{Im}\,\Sigma(\mathbf{k}_F,\omega)$ for $\mathbf{k}_F$ in the (11) direction in units of $t=0.4$ eV.

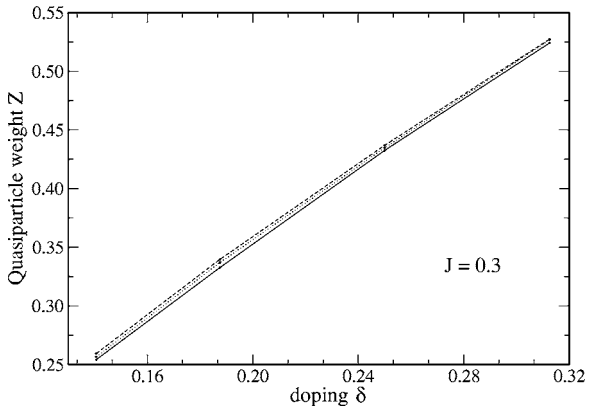

FIG. 8. Quasiparticle weight Z versus doping for the three $\mathbf{k}$ points on the FS discussed in Fig. 7. As discussed in the text there is no indication of the proximity to the DDW phase. The calculations run from $\delta>\delta_c\sim 0.14$ where the HFL is stable.

Inset of Fig. 7 shows a plot of $-\mathrm{Im}\,\Sigma(\mathbf{k}_F,\omega)$ for $\omega<0$ for $\mathbf{k}_F$ in the (11) direction. We have used $t=0.4$ eV.[3] In the range $-200\ \mathrm{meV}<\omega<0$, $-\mathrm{Im}\,\Sigma(\mathbf{k},\omega)$ does not saturate as in Fig. 1 of Ref. 20. The lack of saturation of $-\mathrm{Im}\,\Sigma(\mathbf{k},\omega)$, up to an energy scale of the order of -200 (-300) meV, is well established in cuprates and clearly it cannot be explained by phonons. In addition to this feature, Fig. 1 of Ref. 20 shows the presence of an additional energy scale of the order of 60–70 meV which is associated with the kink observed in ARPES.[3] This small energy scale is not seen in our $-\mathrm{Im}\,\Sigma(\mathbf{k},\omega)$. Whether the kink is due to magnetic excitations or additional degrees of freedom like phonons is still controversial.[3,24] For instance, Yunoki *et al.*,[22] using variational MC simulations, found no evidence for the kink in the context of the pure t-J model and, on the other hand, FLEX calculations for the Hubbard model suggest that the interaction between QP and spin fluctuations leads to the kink (see Ref. 25 and references therein). As mentioned in previous sections the PIH approach weakens spin fluctuations compared to charge fluctuations which means that $1/N^2$ self-energy corrections should be calculated in order to study the kink, if originated by magnetic excitations.

Finally, as expected from the results shown in the top and middle panels, the bottom panel of Fig. 7 shows that, for the three mentioned $\mathbf{k}$ vectors, the corresponding spectral functions are isotropic.

As shown in Ref. 11, in agreement with previous calculations,[26–28] for $J=0.3$, the system presents a flux phase (FP) [also called a d density wave[29] (DDW)] for $\delta<\delta_c\sim 0.14$. The FP was interpreted as a candidate for the pseudogap phase of cuprates.[28,29] Thus, it is important to study self-energy corrections approaching the FP instability from the HFL phase ($\delta\to\delta_c$ from above). Similar calculations to those for $\delta=0.3$ show, for $\delta\gtrsim\delta_c\sim 0.14$, isotropic self-energy effects on the FS.

Figure 8 shows Z versus δ for three $\mathbf{k}$ points chosen as in Fig. 7, each one of them on its corresponding FS for each

doping. Results are for $\delta < 0.3$. The QP weight is very isotropic on the FS even for doping near δ_c. According to our results the anisotropy between the X point [(10) direction] and nodal point [(11) direction], observed in ARPES spectra in cuprates, cannot be interpreted as originated by self-energy effects. This is close to the recent interpretation by Kaminski *et al.*[30] where the scattering rate was found to be composed of an isotropic inelastic term and a highly anisotropic elastic term which correlates with the anisotropy of the pseudogap. In our case, $\mathrm{Im}\,\Sigma$ can be interpreted as the inelastic contribution to the scattering rate and the opening of the flux phase, which is mainly of static character,[11,28] as the elastic term. (A close comparison with ARPES experiments in cuprates, which needs a better FS as given by the tt'-J model, is in progress.)

It is important to discuss the reason for the lack of strong influence of the flux instability on the self-energy. As discussed in Refs. 11 and 28, the flux phase is mainly of static and d-wave symmetry character and it is weakly coupled to the charge sector. Since our self-energy is dominated by charge fluctuations (see below), Σ does not strongly prove the proximity to the DDW. In terms of Ref. 29, the proximity to the DDW is hidden for the one-particle spectral densities. This is in contrast with the self-energy behavior in the proximity of the usual charge density wave (CDW) instability. In Ref. 14 it was shown that the QP weight Z is strongly affected when the system approaches the CDW phase.

A discussion about the excitations that, interacting with electrons, cause the self-energy renormalizations is necessary. In the usual many-body language, the self-energy can be expressed in terms of the relevant quantity $\alpha^2F(\omega)$,[31] where the notation is chosen in a way such that $F(\omega)$ gives information on the density of states of a boson interacting with the electrons, and α^2 about the coupling. In the usual metals, $\alpha^2F(\omega)$ contains information about the electron-phonon interaction averaged over the FS. For simplicity, we will discuss the $J=0$ case. Equation (17) is conveniently written for finding $\alpha^2F(\omega)$. In the first term of the right-hand side of Eq. (17) we can interpret $B^{RR}=-2\,\mathrm{Im}\,D_{RR}$ as the spectral function of the boson mediating the interaction, and the remaining squared factor Ω^2 as the coupling. As discussed in Sec. II D_{RR} corresponds to the charge-charge correlation function [Eq. (9)].

Figure 9 shows $\alpha^2F(\omega)$ obtained from the first term of Eq. (17). Following the discussion above, $\alpha^2F(\omega)$ is proportional to the average on the FS of the charge densities. Clearly, charge density survives up to high energy causing large self-energy effects at large ω. Since charge densities, in $O(1)$, present collective peaks at the top of the particle-hole continuum[11] both the collective excitations and the continuum contribute to $\alpha^2F(\omega)$. For instance, the pronounced structure at $\omega \sim \pm 1.7$ in Fig. 9 is mainly due to collective fluctuations. The interpretation of the last two terms of the right-hand side of Eq. (17) is less direct and they are part of our strong coupling perturbative approach. However, they are also dominated by collective excitation of charge character arising from the inversion of the matrix D.

Sum rule. Before closing we will discuss the spectral function sum rule $\int d\omega\, A(\mathbf{k},\omega)$. In the framework of the t-J model the sum rule is $\langle X^{00}\rangle + \langle X^{\sigma\sigma}\rangle = (1+\delta)/2$. Using the relation $X^{0\sigma} = \sqrt{Nr_0} f_p$, in the limit $N=2$, our sum rule is $\delta(\langle X^{00}\rangle)$; therefore, the PIH method misses a contribution $\langle X^{\sigma\sigma}\rangle = (1-\delta)/2$, making the situation better for large than for low doping. It is important to discuss the possible origin of this discrepancy. As was pointed out in previous papers,[32,33] in order to guarantee the commutation rules for X operators not all the multiplication rules can be satisfied. For instance, in Ref. 32 we have studied the spin system using the four X operators $X^{\sigma\sigma'}$ and showed that the formulation leads to the well-known coherent-state path integral representation for spins.[34] The fact that this representation is better for large than for small S (Ref. 34) was understood, in Ref. 32, as a consequence of the fact that not all the multiplication rules are satisfied. It is worth noting that the formalism in Ref. 32 reproduces the spinless fermion case when the rules are written using X-operator representation. In the present case we deal with the t-J model and in order to satisfy the commutation rules, the formalism requires the constraint $X^{\sigma 0}X^{0\sigma'} = X^{00}X^{\sigma\sigma'}$,[9,33] which reproduces the exact multiplication rule $X^{\sigma 0}X^{0\sigma'} = X^{\sigma\sigma'}$ in the limit $X^{00} \to 1$ ($\delta \to 1$), making the representation better for large than for low doping. In mathematical terms, our expansion seems to be appropriate for both large N and large δ. This is closely related to the fact that the formulation weakens spin compared to charge fluctuations. The band narrowing, discussed in Sec. IV, is possibly connected with this discussion if a spin term $\langle X^{\sigma\sigma}\rangle$ also contributes to the bandwidth. The solution of this very hard theoretical problem, and the knowledge of how important is its effect as a function of doping on different physical quantities, requires not only an effort on the formal level, but also, at the same time, confronting results obtained with different methods.

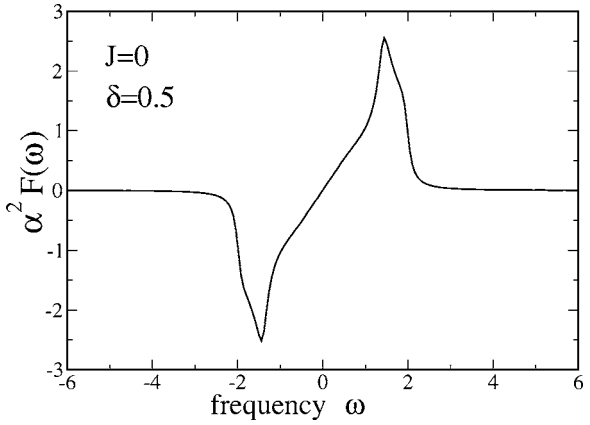

FIG. 9. $\alpha^2F(\omega)$ as extracted from Eq. (17) for Σ. As discussed in the text, $\alpha^2F(\omega)$ is mainly dominated by collective excitations of the charge character. The frequency ω and α^2F are in units of t.

VI. DISCUSSIONS AND CONCLUSIONS

The recently developed path integral large-N approach for Hubbard operators, the PIH method, was used for calculating self-energy corrections and spectral functions, including

fluctuations above the mean-field solution of the t-J model.

Similarities and differences compared to the SB method were discussed in Sec. III. To gain confidence in our calculation, comparisons of spectral functions with Lanczos results for $J=0.3$ and for doping $\delta=0.75$, 0.5, and 0.3125 were performed in Sec. IV. We found fair agreement for each $\mathbf{k}$ on the BZ. PIH self-energies and spectral functions for different J and δ have been investigated in Sec. V. The general characteristics of the self-energy are the following.

(a) Around $\omega=0$, $\mathrm{Im}\,\Sigma(\omega)\sim\omega^2$ which is characteristic of a FL behavior. This is in agreement with the negative slope of $\mathrm{Re}\,\Sigma(\omega)$ at $\omega=0$.

(b) $\Sigma(\omega)$ is very asymmetric with respect to $\omega=0$, indicating the difference between addition and removal of one electron in a strongly correlated system.

(c) $\Sigma(\omega)$ has large structures at large negative ω of the order of a few t.

For $J=0$, we have shown that Z decreases monotonically as $\delta\rightarrow 0$, remaining finite for $\delta>0$. For small δ, $Z\sim 1.4\delta$. As expected, in the uncorrelated limit, $Z\rightarrow 1$ for $\delta\rightarrow 1$.

We have also studied spectral functions along the FS for different δ and $J=0.3$. For this case, the HFL is unstable against a DDW phase for doping $\delta<\delta_c\sim 0.14$. Since the DDW phase was interpreted as a candidate for describing the pseudogap state in cuprates, we have studied the behavior of the self-energy along the FS when approaching the DDW instability. It has been found that self-energy effects and spectral functions are very isotropic along the FS even for doping close to δ_c.

In Sec. V we have discussed the nature of the excitations that, interacting with the charge carriers, produce the self-energy renormalizations. Charge excitations, dominated by collective effects, are the main contribution to $\alpha^2F(\omega)$. As collective charge fluctuations exist on a large energy scale, they are responsible for the large self-energy effects at large energy, producing reduction of the quasiparticle weight and transferring spectral weight to the incoherent spectra at large binding energy.

The PIH method seems to be a suitable alternative for calculating spectral functions in the t-J model; moreover it can be used independently or as a complement to other calculations as well.

ACKNOWLEDGMENTS

We thank L. Manuel, J. Merino, A. Muramatsu, A. Trumper, and R. Zeyher for stimulating discussions and H. Parent for critical reading of the manuscript.

[1] J. G. Bednorz and K. A. Müller, Z. Phys. B: Condens. Matter **64**, 189 (1986).
[2] P. W. Anderson, *The Theory of Superconductivity in High-T_c Cuprates* (Princeton University Press, Princeton, NJ, 1997).
[3] A. Damascelli, Z.-X. Shen, and Z. Hussain, Rev. Mod. Phys. **75**, 473 (2003).
[4] G. Martinez and P. Horsch, Phys. Rev. B **44**, 317 (1991).
[5] A. Izyumov, Phys. Usp. **40**, 445 (1997).
[6] M. Brunner, F. Assaad, and A. Muramatsu, Phys. Rev. B **62**, 15480 (2000).
[7] E. Dagotto, Rev. Mod. Phys. **66**, 763 (1994).
[8] J. Jaklic and P. Prelovsek, Adv. Phys. **49**, 1 (2000).
[9] A. Foussats and A. Greco, Phys. Rev. B **65**, 195107 (2002).
[10] E. Arrigoni, C. Castellani, M. Grilli, R. Raimondi, and G. Strinati, Phys. Rep. **241**, 291 (1994).
[11] A. Foussats and A. Greco, Phys. Rev. B **70**, 205123 (2004).
[12] Z. Wang, Int. J. Mod. Phys. B **6**, 155 (1992).
[13] R. Zeyher and M. L. Kulić, Phys. Rev. B **53**, 2850 (1996).
[14] J. Merino, A. Greco, R. H. McKenzie, and M. Calandra, Phys. Rev. B **68**, 245121 (2003).
[15] A. Greco, J. Merino, A. Foussats, and R. H. McKenzie, Phys. Rev. B **71**, 144502 (2005).
[16] Z. Wang, Y. Bang, and G. Kotliar, Phys. Rev. Lett. **67**, 2733 (1991).
[17] L. Gehlhoff and R. Zeyher, Phys. Rev. B **52**, 4635 (1995).
[18] We thank J. Riera for useful discussions and for his Lanczos programs.
[19] W. Stephan and P. Horsch, Phys. Rev. Lett. **66**, 2258 (1991).
[20] X. J. Zhou, T. Yoshida, A. Lanzara, P. Bogdanov, S. Kellar, K. Sherr, W. Yang, F. Ronning, T. Sasagawa, T. Kakeshita, T. Noda, H. Eisaki, S. Uchida, C. Lin, F. Zhou, J. Xiong, W. Ti, Z. Zhao, A. Fujimori, Z. Hussain, and Z.-X. Shen, Nature (London) **423**, 398 (2003).
[21] J. Fink, S. Borisenko, A. Kordyuk, A. Koitzsch, J. Geck, V. Zabolotnyy, M. Knupfer, B. Büchner, and H. Berger, cond-mat/0512307 (unpublished).
[22] S. Yunoki, E. Dagotto, and S. Sorella, Phys. Rev. Lett. **94**, 037001 (2005)
[23] T. Yoshida, X. J. Zhou, T. Sasagawa, W. L. Yang, P. V. Bogdanov, A. Lanzara, Z. Hussain, T. Mizokawa, A. Fujimori, H. Eisaki, Z.-X. Shen, T. Kakeshita, and S. Uchida, Phys. Rev. Lett. **91**, 027001 (2003).
[24] R. Zeyher and A. Greco, Phys. Rev. B **64**, 140510(R) (2001).
[25] D. Manske, *The Theory of Unconventional Superconductors* (Springer-Verlag, Berlin, 2004).
[26] I. Affleck and J. B. Marston, Phys. Rev. B **37**, 3774 (1988).
[27] D. C. Morse and T. C. Lubensky, Phys. Rev. B **42**, 7994 (1990).
[28] E. Cappelluti and R. Zeyher, Phys. Rev. B **59**, 6475 (1999).
[29] S. Chakravarty, R. B. Laughlin, D. K. Morr, and Ch. Nayak, Phys. Rev. B **63**, 094503 (2001).
[30] A. Kaminski, H. M. Fretwell, M. R. Norman, M. Randeria, S. Rosenkranz, U. Chatterjee, J. C. Campuzano, J. Mesot, T. Sato, T. Takahashi, T. Terashima, M. Takano, K. Kadowaki, Z. Z. Li, and H. Raffy, Phys. Rev. B **71**, 014517 (2005).
[31] G. Mahan, *Many-Particle Physics* (Plenum Press, New York, 1981).
[32] A. Foussats, A. Greco, and O. S. Zandron, Ann. Phys. (N.Y.) **275**, 238 (1999); **279**, 263 (2000).
[33] A. Foussats, A. Greco, C. Repetto, O. P. Zandron, and O. S. Zandron, J. Phys. A **33**, 5849 (2000).
[34] E. Fradkin, *Field Theories of Condensed Matter Systems* (Addison-Wesley, Reading, MA, 1991).